journal

J. Am. Ceram. Soc., 98 [1] 186–189 (2015)
DOI: 10.1111/jace.13266

Strain-Dependent Plasticity Evolution of Window Glass

Dong-Hyun Lee, In-Chul Choi, Moo-Young Seok, Yakai Zhao, Jung-A Lee, and Jae-il Jang†

Division of Materials Science and Engineering, Hanyang University, Seoul 133-791, South Korea

How the applied strain can affect the plasticity evolution of window glass was systematically explored through a series of nanoindentations with various sharp indenters. It was revealed that, as the strain increases, the contribution of shear flow to total plasticity becomes larger, whereas that of densification gets smaller. The results are discussed in terms of the sequence in which each mechanism plays and the detailed mechanism of shear flow.

I. Introduction

Conventional oxide glasses are brittle at ambient temperature and fail in a catastrophic manner under tensile or bending stresses. However, it has been reported that they can show a considerable plasticity under a certain mechanical environment since Taylor's first report in 1949 that indentation with a sharp indenter lefts permanent impression on the glass surface.[1] Due to the absence of crystalline defects such as dislocations, the mechanism of the plastic deformation in oxide glasses should be different from that in crystalline ceramics. The possible mechanism found earliest was densification, that is, a permanent volume contraction under compressive stresses.[2] This is possible because amorphous materials have more open structure than chemically equivalent crystals and the structure can be condensed into a more close-packed arrangement by external loading.[3] The densified region is known to be recovered by annealing treatment.[4] The fact that apparent activation energy of the recovery in the indented glass is close to that in hydrostatically densified glass[5] suggests that the densification plays an important role in the plastic deformation underneath a indenter possibly due to the existence of indentation core under hydrostatic pressure.[6] The extent of densification varies with glass composition, especially concentration of network modifiers such as Na_2O or CaO[7,8]; glasses having more modifiers exhibit smaller densification, because the modifiers occupy the free space which can shrink by external stress.

In 1970, Peter[7] argued that the permanent densification cannot fully explain indentation behavior of oxide glasses; for example, the presence of material pile-up around hardness impression and the slip lines below the indentation indicates that there is also some contribution of shear flow to the indentation-induced plasticity.[7,9–11] Now, it is well accepted that plastic deformation in oxide glasses is caused by both densification and shear flow. Nevertheless, how the contribution of each mechanism can be affected by mechanical environment is not yet fully understood. Especially, only limited efforts have been made for analyzing the contribution of shear flow.

A good first step for addressing this issue can be to analyze the influence of applied strain on the contribution of each mechanism to the indentation-induced plasticity. With continuum mechanics concept, the strains underneath a sharp indenter are unique and independent of indentation load or displacement due to the so-called geometrical self-similarity of the sharp tip. A way to overcome this difficulty in applying different strain is varying the sharpness of indenter. Generally, sharper indenters with smaller indenter angles induce larger strains in the material due to the larger volume of displaced material.[12–15] The indenter sharpness dependency of deformation mechanism in metallic materials has been previously reported.[16,17] With this in mind, here we systematically explore how the applied strain affect the indentation-induced plasticity evolution of window glass (soda-lime silicate glass) through a series of nanoindentation tests using five different three-sided pyramidal indenters having a variety of sharpness.

II. Experimental Procedure

Nanoindentation tests were performed on a commercial window glass using a Nanoindenter-XP (formerly MTS; now Agilent, Oak Ridge, TN) with five different three-sided pyramidal indenters having a centerline-to-face angle ψ of 35.3° (cube-corner indenter), 50°, 65.3° (Berkovich indenter), 75°, and 85°. The sample was loaded to the maximum load, P_{max}, at a constant loading rate, dP/dt, of 10 mN/s. More than 30 tests were performed for each condition. To support the analysis of the sharp indentations, nanoindentations with a spherical tip (whose radius, R, was determined as 6.38 μm by Hertzian contact analysis[18]) were additionally made at 50 and 75 mN.

The indented samples were annealed at 753 K (~$0.9T_g$ where T_g is the glass transition temperature) for 2 h in an electric furnace. Based on previous reports,[4,8] one may expect that this annealing condition allows a nearly complete recovery of the densified region, and only the shear flow contribution remains after the annealing. Before and after annealing, hardness impression morphologies were imaged using both a field-emission scanning electron microscopy (FE-SEM), JSM-6330F (JEOL Ltd., Tokyo, Japan), and an atomic force microscopy (AFM), XE-100 (Park System, Suwon, Korea). Prior to taking SEM images, thin gold coating was applied to the indented surface to avoid charging.

III. Results and Discussion

Figure 1 shows representative load-displacement (P–h) curves from nanoindentations made with various indenters. As one may expect, maximum h (h_{max}) increases with decreasing ψ (or increasing sharpness). While the indenter having ψ = 85° exhibits purely elastic contact, as evidenced by the fact that the loading and unloading curves are identical, all other indenters (ψ = 35.3°, 50°, 65.3°, and 75°) left the residual h (h_r) after unloading. Difference in the ratio of h_r/h_{max} for each indenter (e.g., ~0.747 for 35.3° and ~0.253 for 75°) indicates that indeed different level of plastic deformation occurs in the window glass.

T. Rouxel—contributing editor

Manuscript No. 35159. Received June 16, 2014; revised September 1, 2014; approved September 2, 2014.
†Author to whom correspondence should be addressed. e-mail: jijang@hanyang.ac.kr

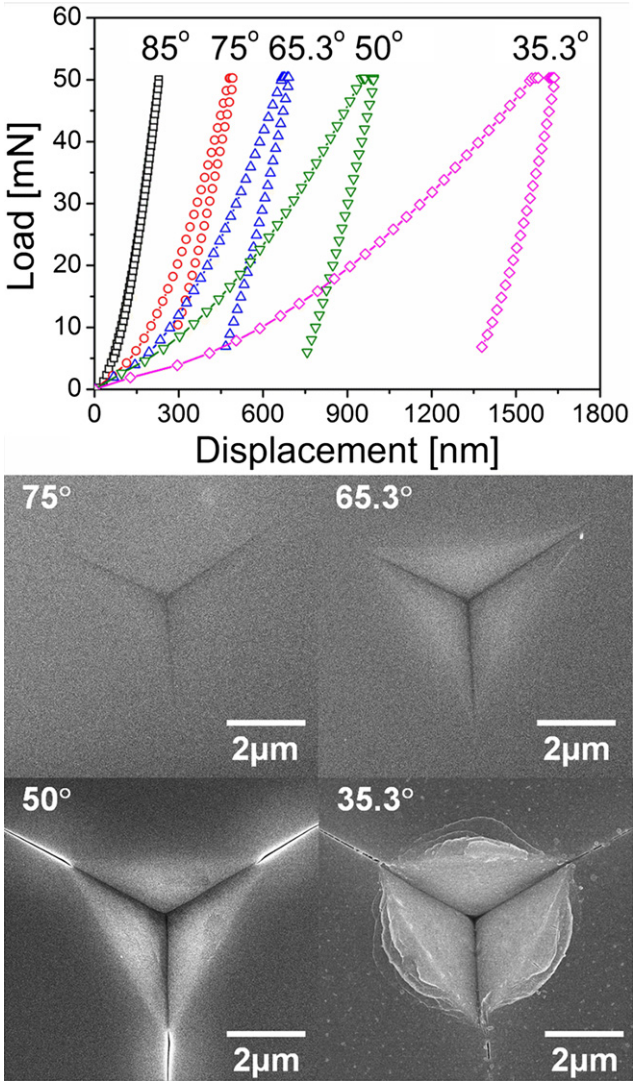

Fig. 1. Representative *P–h* curves (P_{max} = 50 mN) and hardness impressions (P_{max} = 100 mN) obtained during nanoindentations with different indenters. The hardness impression was obtained at a higher load for clearer observations. Note that the magnification of each SEM image is not the same.

Figure 1 also exhibits typical SEM images of hardness impression obtained at 100 mN, a higher load for more clear observations. No image is provided for $\psi = 85°$ since its contact is purely elastic. The morphology of the impression is significantly varied with ψ: The edge of contact is unclear for $\psi = 75°$ and becomes a little clearer (but not fully clear yet) for $\psi = 65.3°$. This uncertainty is expected due to the shallow depth of the indentations. For $\psi = 50°$, the contact edge is very clear and well-developed radial cracks are observed in each corner. Finally, for $\psi = 35.3°$, pronounced indentation pile-up behavior with shear banding occurs around the impression, which is the evidence for the large contribution of shear flow to the total plasticity.

The influence of ψ on each contribution of densification and shear flow was examined by analyzing the AFM surface profiles of the hardness impressions taken before and after annealing. Inset of Fig. 2 provides extreme cases of $\psi = 35.3°$ and 75°. Two important features can be captured: First, annealing-induced change in the indent morphology due to the recovery of densification is much more pronounced for $\psi = 75°$ than for 35.3°. Oppositely, second, material pile-up around indentation (which may be an evidence of shear flow) is much more developed for $\psi = 35.3°$ than for 75°. For quantitative evaluation of densification and shear flow, pile-up height, $h_{pile\text{-}up}$, and the residual h before

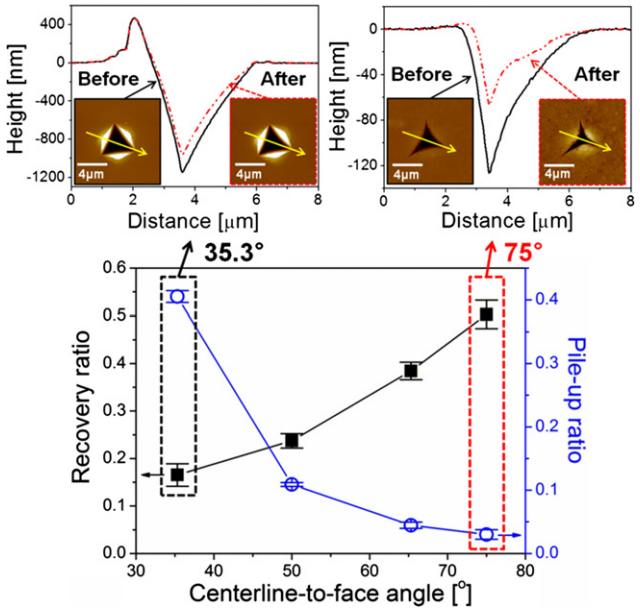

Fig. 2. Representative AFM data (for $\psi = 35.3°$ and 75°) and the variations in recovery ratio and pile-up ratio as a function of indenter angle.

and after annealing (h_r^b and h_r^a, respectively) were measured from the AFM data. Both recovery ratio, $(h_r^b - h_r^a)/h_r^b$, and pile-up ratio, $h_{pile\text{-}up}/h_r^b$, (which is an indicator for the contribution of densification and shear flow to total plasticity, respectively) are calculated and summarized as function of ψ in Fig. 2. As ψ is reduced (or sharpness is increased), recovery ratio decreases and pile-up ratio increases. Additionally, annealing-induced changes in the indentation volume (V_{indent}) and pile-up volume ($V_{pile\text{-}up}$) were estimated by the AFM software. From the data, both recovery ratio of indentation volume, $V_R = \{(V_{indent}^b - V_{indent}^a) + (V_{pile\text{-}up}^a - V_{pile\text{-}up}^b)\}/V_{indent}^b$, and ratio of pile-up volume, $V_P = V_{pile\text{-}up}/V_{indent}^b$, were calculated as summarized in Table I. As one might expect, the trends in Fig. 2 and Table I are quite similar. From this, one may gain an insight for the effect of indenter sharpness on densification and shear flow, that is, during indentation with a sharper tip, the contribution of shear flow becomes larger, whereas that of densification becomes smaller.

The characteristic (or indentation) strain, ε_{char}, underneath a sharp indenter is independent of h due to its geometrical self-similarity, and the ε_{char} of a conical indenter is commonly determined as[13,19]

$$\varepsilon_{char} = 0.2 \cdot \cot\theta \tag{1}$$

Here, θ is half-cone angle, related to the ψ by

$$\theta = \tan^{-1}\left(\sqrt{\frac{3\sqrt{3}}{\pi}}\tan\psi\right)$$

[15] which is derived under the assumption that similar behavior is obtained when the angle of the cone gives the same area-to-depth ratio as the three-sided pyramid. Thus, $\psi = 35.3°$, 50°, 65.3°, 75°, and 85° would correspond to $\theta = 42.3°$, 56.9°, 70.3°, 78.2°, and 86.1°, respectively. Equation (1) leads to ε_{char} for $\psi = 85°$, 75°, 65.3°, 50°, and 35.3° as 0.014, 0.042, 0.072, 0.13, and 0.22, respectively.

Analysis of the applied ε_{char} effect can be supported by additional indentations using a spherical tip where geometrical self-similarity does not exist. For a spherical indentation, the ε_{char} of Eq. (1) is often redescribed as

Table I. Summary of Indentation and Pile-Up Volumes and Their Changes by Annealing

ψ (°)	$V_{indent}{}^{b}$ (μm^3)	$V_{pile\text{-}up}{}^{b}$ (μm^3)	$V_{indent}{}^{a}$ (μm^3)	$V_{pile\text{-}up}{}^{a}$ (μm^3)	V_R	V_P
35.3	1.995 ± 0.111	1.619 ± 0.222	1.443 ± 0.057	1.639 ± 0.291	0.282 ± 0.084	0.752 ± 0.129
50	0.950 ± 0.018	0.242 ± 0.023	0.598 ± 0.032	0.372 ± 0.093	0.464 ± 0.030	0.163 ± 0.037
65.3	0.462 ± 0.028	0.067 ± 0.004	0.170 ± 0.004	0.106 ± 0.001	0.717 ± 0.014	0.068 ± 0.036
75	0.151 ± 0.007	0.016 ± 0.003	0.037 ± 0.002	0.021 ± 0.001	0.794 ± 0.009	0.064 ± 0.024

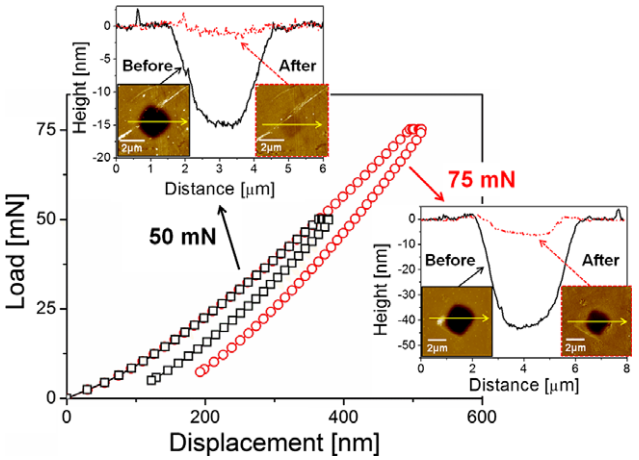

Fig. 3. Representative *P–h* curves of spherical nanoindentations (at P_{max} = 50 and 75 mN). Inset images show the corresponding AFM surface profiles obtained before and after the annealing.

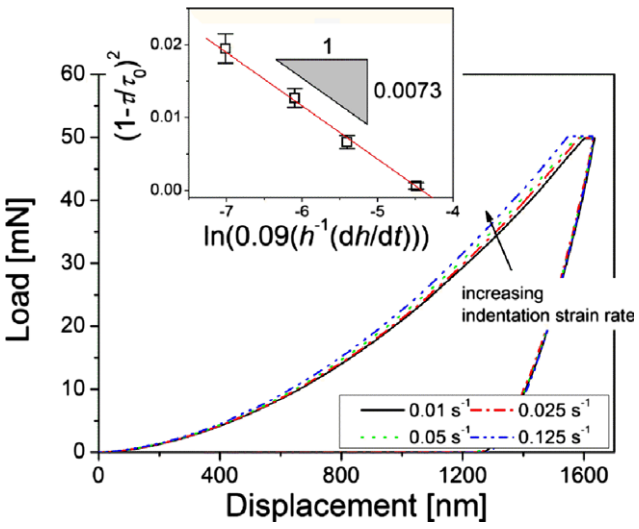

Fig. 4. *P–h* curves of cube-corner indentations obtained at four different indentation strain rates. The influence of the strain rate on the shear flow is provided in the inset.

$$\varepsilon_{char} = 0.2\frac{a}{R} \tag{2}$$

where a is the contact radius and R is the radius of spherical tip.[19,20] The value of a can be calculated by putting the contact depth h_c (given by $h_c = h - \omega\frac{P}{S}$[18] where S is the contact stiffness and ω is a geometric constant of 0.75 for sphere) into the contact geometry equation $a^2 = 2Rh_c - h_c^2$.[20] Thus, the ε_{char} for spherical tip can be systematically varied by simply changing P (and thus a). For this purpose, nanoindentations with a spherical tip (having R = 6.38 μm) were conducted at 50 and 75 mN, and their *P–h* curves and AFM data are shown in Fig. 3. It is obvious that annealing-induced change in the indent morphology depends on P_{max}. While almost complete recovery was observed for P_{max} = 50 mN, the annealing could not fully recover the impression for 75 mN. This provides a clue for the sequence in which each mechanism plays; that is, plastic deformation at the early stage is primarily caused by densification, and then shear flow starts to contribute at higher strain level. Considering that there is saturation level of densification in the glasses,[6,21] it can be suggested that once saturation of densification is achieved, additional plasticity should be accommodated by means of shear flow.

According to Eq. (2), the values of ε_{char} for the spherical indentations (in Fig. 3) were calculated as 0.059 and 0.063 for P_{max} = 50 and 75 mN, respectively. Therefore, it is reasonable to believe that saturation of densification is reached between ε_{char} of 0.059 and 0.063. In sharp indentation, since ε_{char} for ψ = 65.3° (~0.072) is higher than 0.063, the saturation level of densification is already reached and shear flow plays nonnegligible role in the deformation. Thus, the increase in ε_{char} with reducing ψ can explain the variations in the contribution of shear flow in Fig. 2, and the contribution of the shear flow becomes the largest for ψ = 35.3° due to its highest ε_{char} (~0.22). Note that, although ε_{char} for ψ = 75° (~0.042) is lower than 0.059, there is still a possibility of small role of shear flow due to the stress singularity of tip.[22]

An important issue remaining unclear yet is the detailed mechanism for the shear flow. In the absence of dislocation, Argon suggested that the shear flow in both metallic and ceramic glasses is the result from a succession of localized structural rearrangements.[23,24] Especially in oxide glasses, it was proposed that the local rearrangement proceeds through a shear transformation (that is, a complex and cooperative internal exchange of atoms) in a roughly equiaxed region. In this theory, strain-rate ($\dot{\varepsilon}$) dependence of shear stress (τ) can be given by[24]:

$$\left(1 - \frac{\tau}{\tau_0}\right)^2 = \frac{4(1-B)kT}{\tau_0\Omega\gamma_0} \cdot (\ln\alpha\gamma_0\nu_G - \ln\dot{\varepsilon}) \tag{3}$$

Here, τ_0 is the threshold plastic resistance at a given absolute temperature T, k is the Boltzmann constant, Ω is the volume of shear transformation zone, γ_0 is the transformation shear strain, ν_G is the normal mode frequency of the transforming complex along the activation path, α is a constant related to the fraction of material that is available to deform via the activated process, and B is the scale factor of the modified elastic energy stored around the transformed region that can be determined as

$$B = \frac{(7-5\nu)}{30(1-\nu)} \cdot \frac{G\gamma_0}{\tau_0} \tag{4}$$

where ν is the Poisson's ratio (~0.23) and G is the shear modulus (~30.1 GPa). If the above suggestion by Argon[24] holds valid for the shear flow observed in this study, the data of cube-corner indentations (ψ = 35.3°), which exhibits the largest contribution of the shear flow, should fit well with Eq. (3). To examine this, a series of cube-corner indentations were performed under four different indentation strain rate $\dot{\varepsilon}_i = h^{-1}(dh/dt)$ of 0.01, 0.025, 0.05, and 0.125 s^{-1}. The representative *P–h* curves recorded during the tests are

provided in Fig. 4 where obvious rate dependence is observed; that is, h_{max} decreases as $\dot{\varepsilon}_i$ increases. At a given $\dot{\varepsilon}_i$, hardness H was estimated according to Oliver-Pharr (O-P) method.[18] In the estimations by O-P method, two points are noteworthy. First, the value of correlation constant β (that relates stiffness S to contact area) is validated only for a Berkovich indenter ($\psi = 65.3°$) and not for any other ψ. Thus, here β for $\psi = 35.3°$ was assumed to be 1.097 following a previous study on fused quartz.[25] Second, estimated H values may be overestimated due to its pronounced pile-up behavior for $\psi = 35.3°$.

From H, the τ in Eq. (3) can be determined by von Mises conversion of flow stress σ and the well-known Tabor's relation,[20] $\tau \approx \frac{\sigma}{\sqrt{3}9} \approx \frac{H}{\sqrt{3}C}$ where C is the constraint factor (~1.4 for window glass[9]). In addition, the strain rate for uniaxial loading $\dot{\varepsilon}$ can be obtained by an empirical relation of $\dot{\varepsilon} \approx 0.09\dot{\varepsilon}_i$.[26] Then, one can draw the plot of $(1 - \tau/\tau_0)^2$ versus $\ln\dot{\varepsilon}$ as shown in the inset of Fig. 4 in which indeed the experimental data are in good agreement with the theoretical predictions by Eq. (3). From the slope of the plot, the value of Ω can be directly determined as 3.014 nm^3 with the assumptions of $\tau_0 = G/2\pi$ (as predicted from a sinusoidal shear resistance) and $\gamma_0 = 0.125$ (as for metallic glasses[23,24]). Reasonable agreement between our Ω and literature data (~1.5 nm^3)[24] led us to conclude that shear flow in the examined window glass is mainly due to the shear transformation in a roughly equiaxed region.

IV. Conclusions

In summary, we have explored the influence of applied strain (or indenter sharpness) on the plastic deformation behavior of window glass through a series of nanoindentation experiments with five different three-sided pyramidal indenters. Experimental results revealed that, as the sharpness (and strain) increases, the contribution of shear flow to total plasticity becomes larger, whereas that of densification gets smaller. Detailed sequence in which each mechanism plays could be determined by additional nanoindentations with a spherical indenter. The strain-rate dependency of the cube-corner indentation data suggested that the shear flow in the examined window glass results from a shear transformation.

Acknowledgments

This research was supported in part by the National Research Foundation of Korea (NRF) grant funded by the Korea government (MSIP) (no. 2013R1A1A2A10058551), and in part by the Human Resources Development program of the Korea Institute of Energy Technology Evaluation and Planning (KETEP) grant funded by the Korea government (MOTIE) (no. 20134030200360).

References

[1]E. W. Taylor, "Plastic Deformation of Optical Glass," *Nature*, **163**, 323 (1949).

[2]F. M. Ernsberger, "Role of Densification in Deformation of Glasses Under Point Loading," *J. Am. Ceram. Soc.*, **51**, 545–7 (1968).

[3]J. Zarzycki, *Glasses and the Vitreous State*. Cambridge University Press, Cambridge, 1991.

[4]J. D. Mackenzie, "High-Pressure Effects on Oxide Glass: II, Subsequent Heat Treatment," *J. Am. Ceram. Soc.*, **46**, 470–6 (1963).

[5]J. E. Neely and J. D. Mackenzie, "Hardness and Low-Temperature Deformation of Silica Glass," *J. Mater. Sci.*, **3**, 603–9 (1968).

[6]H. Ji, V. Keryvin, T. Rouxel, and T. Hammouda, "Densification of Window Glass Under Very High Pressure and Its Relevance to Vickers Indentation," *Scripta Mater.*, **55**, 1159–62 (2006).

[7]K. W. Peter, "Densification and Flow Phenomena of Glass in Indentation Experiments," *J. Non-Cryst. Solids*, **5**, 103–15 (1970).

[8]S. Yoshida, J.-C. Sanglebœuf, and T. Rouxel, "Quantitative Evaluation of Indentation-Induced Densification in Glass," *J. Mater. Res.*, **20**, 3404–12 (2005).

[9]J. T. Hagan, "Shear Deformation Under Pyramidal Indentations in Soda-Lime Glass," *J. Mater. Sci.*, **15**, 1417–24 (1980).

[10]B. R. Lawn, T. P. Dabbs, and C. J. Fairbanks, "Kinetics of Shear-Activated Indentation Crack Initiation in Soda-Lime Glass," *J. Mater. Sci.*, **18**, 2785–97 (1983).

[11]B. R. Lawn and R. F. Cook, "Probing Material Properties with Sharp Indenters: A Retrospective," *J. Mater. Sci.*, **47**, 1–22 (2012).

[12]J.-i. Jang, M. J. Lance, S. Wen, T. Y. Tsui, and G. M. Pharr, "Indentation-Induced Phase Transformations in Silicon: Influence of Load, Rate, and Indenter Angle on the Transformation Behavior," *Acta Mater.*, **53**, 1759–70 (2005).

[13]S. Shim, J.-i. Jang, and G. M. Pharr, "Extraction of Flow Properties of Single Crystal Silicon Carbide by Nanoindentation and Finite Element Simulation," *Acta Mater.*, **56**, 3824–32 (2008).

[14]J.-i. Jang, B.-G. Yoo, and J.-Y. Kim, "Rate-Dependent Inhomogeneous-to-Homogeneous Transition of Plastic Flows During Nanoindentation of Bulk Metallic Glasses: Fact or Artifact?" *Appl. Phys. Lett.*, **90**, 211906 (2007).

[15]J.-i. Jang, B.-G. Yoo, Y.-J. Kim, J.-H. Oh, I.-C. Choi, and H. Bei, "Indentation Size Effect in Bulk Metallic Glass," *Scripta Mater.*, **64**, 753–6 (2011).

[16]I.-C. Choi, Y.-J. Kim, Y. M. Wang, U. Ramamurty, and J.-i. Jang, "Nanoindentation Behavior of Nanotwinned Cu: Influence of Indenter Angle on Hardness, Strain Rate Sensitivity and Activation Volume," *Acta Mater.*, **61**, 7313–23 (2013).

[17]D.-H. Lee, J.-A. Lee, M.-Y. Seok, U. B. Baek, S. H. Nahm, and J.-i. Jang, "Stress-Dependent Hardening-to-Softening Transition of Hydrogen Effects in Nanoindentation of a Linepipe Steel," *Int. J. Hydrogen Energy*, **39**, 1897–902 (2014).

[18]W. C. Oliver and G. M. Pharr, "Measurement of Hardness and Elastic Modulus by Instrumented Indentation: Advances in Understanding and Refinements to Methodology," *J. Mater. Res.*, **19**, 3–20 (2004).

[19]K. L. Johson, "The Correlation of Indentation Experiments," *J. Mech. Phys. Solids*, **18**, 115–26 (1970).

[20]I.-C. Choi, B.-G. Yoo, Y.-J. Kim, M.-Y. Seok, Y. M. Wang, and J.-i. Jang, "Estimating the Stress Exponent of Nanocrystalline Nickel: Sharp vs. Spherical Indentation," *Scripta Mater.*, **65**, 300–3 (2011).

[21]V. Keryvin, J.-X. Meng, S. Gicquel, J.-P. Guin, L. Charleux, J.-C. Sanglebœuf, P. Pilvin, T. Rouxel, and G. L. Quillie, "Constitutive Modeling of the Densification Process in Silica Glass Under Hydrostatic Compression," *Acta Mater.*, **62**, 250–7 (2014).

[22]S. Yoshida, H. Sawasato, T. Sugawara, Y. Miura, and J. Matsuoka, "Effects of Indenter Geometry on Indentation-Induced Densification of Soda-Lime Glass," *J. Mater. Res.*, **25**, 2203–11 (2010).

[23]A. S. Argon, "Plastic Deformation in Metallic Glasses," *Acta Metall.*, **27**, 47–58 (1979).

[24]A. S. Argon, "Inelastic Deformation and Fracture in Oxide, Metallic, and Polymeric Glasses"; Chapter 3 in *Glass: Science and Technology*, Vol. 5; Edited by D. R. Uhlmann and N. J. Kreidl. Academic Press, New York, NY, 1980.

[25]J. H. Strader, S. Shim, H. Bei, W. C. Oliver, and G. M. Pharr, "An Experimental Evaluation of the β Constant Relating the Contact Stiffness to the Contact Area in Nanoindentation," *Philos. Mag*, **86**, 5285–98 (2006).

[26]W. H. Poisl, W. C. Oliver, and B. D. Fabes, "The Relationship Between Indentation and Uniaxial Creep in Amorphous Selenium," *J. Mater. Res.*, **10**, 2024–32 (1995). □